Top quark pair production cross-section in proton-proton collisions at √s = 7 TeV

Tsiakiris, M.

Publication date
2012

Chapter 6

Top-quark pair production cross-section at $\sqrt{s} = 7$ TeV

"Big results require big ambitions."

Heraclitus of Ephesus
c. 535 BC - c. 475 BC

In this chapter we present the measurement of the inclusive production cross-section of top quark-pair events that are produced in 7 TeV center-of-mass energy of proton-proton collisions in the ATLAS detector. For this proton collision energy the theoretical prediction of the cross-section at NNLO approximation gives a value of $164.6^{+11.4}_{-15.8}$ *pb* (see [55]).

The measurement we present here uses the complete 2010 dataset recorded by ATLAS corresponding to a total of 35.3 pb^{-1} of integrated luminosity (see section 4.4.1). The method we develop relies on the identification of the single-lepton $t\bar{t}$ events in the $t\bar{t}(e)$ and $t\bar{t}(\mu)$ final states, however in the final event sample we make no distinction from other leptonically decaying channels that may be seen as signal e.g. $t\bar{t}(\tau)$ or di-leptonic flavors. Therefore, for deriving the cross-section from the number of identified signal events (N_{signal}) we use equation 4.5.1 in the following form:

$$\sigma_{t\bar{t}} = \frac{N_{signal}}{\int \mathcal{L} dt \cdot BR \cdot \epsilon_{t\bar{t}}} \ , \tag{6.0.1}$$

where $\epsilon_{t\bar{t}}$ is the selection efficiency for $t\bar{t}$ events at any of the leptonic final states and BR corresponds to the branching ratio of our signal events. To estimate the branching ratio we take the branching ratio of $W \to \ell\nu_\ell$ decays to be 0.108 per leptonic flavor or 0.324 for all flavors inclusive [53]. This suggests that the hadronically decaying W boson has a total ratio of 0.676. Since we include all but the fully-hadronic $t\bar{t}$ channel, the branching ratio in equation 6.0.1 will be:

$$BR = 1 - 0.676 \cdot 0.676 = 0.543 \ .$$

In section 6.1 we discuss the estimation of parameter $\epsilon_{t\bar{t}}$ and how we utilize the data-driven scale factors. Section 6.2 presents our simultaneous template fit method. We discuss the general formulation of the method and we provide the list of parameters categorized in those which are obtained from the Monte-Carlo and those which are extracted from data-driven methods. We also discuss the constraints we placed in certain parameters. In section 6.3 we validate the method by applying it on the Monte Carlo and we also perform ensemble and linearity tests. In section 6.4 we present the result by applying the method on the collected

Kinematic Region	Selection efficiency (%)	
	μ-channel	e-channel
$N_{j,25} = 3,\ N_{bj,25} = 0$	1.707 ± 0.009	1.216 ± 0.008
$N_{j,25} = 3,\ N_{bj,25} \geq 1$	3.306 ± 0.013	2.430 ± 0.011
$N_{j,25} \geq 4,\ N_{bj,25} = 0$	2.251 ± 0.010	1.634 ± 0.009
$N_{j,25} \geq 4,\ N_{bj,25} \geq 1$	6.612 ± 0.027	4.353 ± 0.021

Table 6.1: *The $t\bar{t}$ selection efficiency for each of the kinematic regions that are used for the cross-section calculations. The numbers are estimated from the Monte Carlo shown in tables 4.8 and 4.9. The notation is explained in section 4.5.1.*

data sample and in section 6.5 we discuss the relevant systematic uncertainties. Lastly, in section 6.6 we present the measurement based on the combination of the $t\bar{t}(\mu)$ and $t\bar{t}(e)$ channels. The necessary extension on the fit formulation is also explained.

6.1 The $\epsilon_{t\bar{t}}$ estimate and data-driven scale factors

The value of the $t\bar{t}$ selection efficiency ($\epsilon_{t\bar{t}}$), present in equation 6.0.1, can be described as the product of all the individual efficiencies of the selection cuts and of the geometrical acceptance of the detector (A_g). We write it in the following way :

$$\epsilon_{t\bar{t}} = \epsilon_{trig} \cdot \epsilon_{\ell,reco} \cdot \epsilon_{\ell,id} \cdot \epsilon_{other} \cdot A_g \tag{6.1.1}$$

where A_g the geometrical acceptance of the detector, ϵ_{trig} is the efficiency of the trigger selection, $\epsilon_{\ell,reco}$ is the efficiency on the lepton reconstruction, $\epsilon_{\ell,id}$ is the efficiency on the lepton identification, ϵ_{other} is the product of all other efficiencies, namely the jet identification and reconstruction as well as the b-jet identification. Typically, the overall $\epsilon_{t\bar{t}}$ value is estimated from Monte Carlo. Using the results shown in tables 4.8 and 4.9 we get the $\epsilon_{t\bar{t}}$ for each of the kinematic regions of interest for this analysis; the results are shown in table 6.1 and the notation of the kinematic regions are explained section 4.5.1. With this approach systematic variations must be taken into account for each of the terms.

Alternatively, estimates for certain terms can also be obtained from the data itself. For this analysis, data-driven methods are used for the trigger (see also section 3.3), and the lepton reconstruction and identification efficiency terms. The results of these calculations can be compared with the equivalent Monte Carlo ones using scale factors:

$$SF = \frac{\epsilon^{data}}{\epsilon^{MC}} \ . \tag{6.1.2}$$

In this case, the $\epsilon_{t\bar{t}}$ can be corrected to the data-driven estimate and can be re-written as follows:

$$\epsilon_{t\bar{t}} = (\epsilon^{MC}_{trig} \cdot \epsilon^{MC}_{\ell,reco} \cdot \epsilon^{MC}_{\ell,id} \cdot \epsilon^{MC}_{other} \cdot A_g) \cdot (SF_{trig} \cdot SF_{\ell,reco} \cdot SF_{\ell,id}) \tag{6.1.3}$$

The terms that are included in the ϵ_{other} are not corrected at this level but instead systematic variations are taken into account; systematics of the method are discussed in section 6.5.

6.1.1 Trigger scale factors

Trigger scale factors are estimated using the tag-and-probe method on $Z \to \ell\ell$ events, where ℓ stands for electrons or muons. The muon tag-and-probe was introduced in chapter 3. For the

electron trigger also $W \to e\nu_e$ events are used. A detailed description of the method and the results corresponding to the dataset used in this analysis is given in [148, 157] for the electron trigger and in [148].

As mentioned already in section 4.4.2, the electron trigger that is used is the `EF_e15_medium`, which shows a 99% efficiency with a plateau at $E_T \geq 20$ GeV. The result on its scale factor is:

$$SF_{trig,e} = 0.995 \pm 0.005(stat. + syst.) \ , \tag{6.1.4}$$

and is taken uniformly in the whole η and ϕ range that is of interest for this analysis.

For the muon, the triggers used are the `EF_mu10_MSonly`, `EF_mu13` and `EF_mu13_tight`, each for a certain period of the data-taking (see section 4.4.2), a single scale factor however is computed for the total of the selected data. Due to the complexity on the geometry of the Muon Spectrometer, disagreements between data and Monte Carlo have been observed especially with respect to different η and ϕ areas. Therefore the scale factor is separated into ten bin regions as shown in table 6.2. The value of the scale factor at each bin is shown in table 6.3. Although a generally good agreement between Monte Carlo and data is observed, namely the value of the scale factor is close to 1, still fluctuations between the regions are observed justifying the separation into different bins.

Bin Name	η **range**	ϕ **range**
EC	$\|\eta\| > 1.05$	-
B1P1	[-1.05,0.60],	[$-\pi$,$5\pi/16$] or [$11\pi/16$,π]
B1P2	[-1.05,0.60] or [-0.60,-0.50] or [-0.50,0.20] or [0.30,0.60]	[$5\pi/16$,$\pi/2$]
B1P3	[-1.05,0.60]	[$\pi/2$,$11\pi/16$]
B2P1	[-0.60,0.60]	[$-\pi$,$5\pi/16$] or [$11\pi/16$,π]
B2P2	[-0.50,-0.40] or [0.20,0.30]	[$5\pi/16$,$\pi/2$]
B2P3	[-0.60,0.60]	[$\pi/2$,$11\pi/16$]
B3P1	[0.60,1.05]	[$-\pi$,$5\pi/16$] or [$11\pi/16$,π]
B3P2	[0.60,1.05]	[$5\pi/16$,$\pi/2$]
B3P3	[0.60,1.05]	[$\pi/2$,$11\pi/16$]

Table 6.2: *The ten bins in $\eta - \phi$ space for which the muon trigger scale factor is estimated. The first columns give a name for each bin for simplicity. See [148]*

6.1.2 Lepton reconstruction and identification scale factors

In a the same way as with the trigger scale factors the lepton reconstruction and identification scale factors are estimated. For both electrons and muons the tag-and-probe technique is used on $Z \to ee$ [148, 160] or $Z \to \mu\mu$ [148] events respectively. For the electrons, the identification efficiency estimation also uses W events [160] which are combined statistically with the Z boson decay events.

The muon scale factor estimates are calculated independently, but are provided as a single number. No kinematic dependence is given and the value of the scale factor is provided uniformly in $\eta - \phi$ coordinates:

$$SF_{\mu,reco,id} = 0.999 \pm 0.002(stat.) + 0.003(syst.) \ . \tag{6.1.5}$$

It is evident that the agreement between data and Monte-Carlo is very good, while the expected uncertainty is also very low.

Bin Name	Scale Factor ($SF_{trig,\mu}$)
EC	$0.987^{+0.001}_{-0.001}$(syst.) ± 0.003(stat.)
B1P1	$1.026^{+0.003}_{-0.002}$(syst.) ± 0.010(stat.)
B1P2	$0.919^{+0.007}_{-0.000}$(syst.) ± 0.017(stat.)
B1P3	$0.952^{+0.002}_{-0.003}$(syst.) ± 0.030(stat.)
B2P1	$1.009^{+0.001}_{-0.002}$(syst.) ± 0.006(stat.)
B2P2	$0.657^{+0.010}_{-0.000}$(syst.) ± 0.050(stat.)
B2P3	$0.906^{+0.000}_{-0.004}$(syst.) ± 0.019(stat.)
B3P1	$1.005^{+0.002}_{-0.003}$(syst.) ± 0.010(stat.)
B3P2	$0.843^{+0.000}_{-0.013}$(syst.) ± 0.053(stat.)
B3P3	$1.046^{+0.011}_{-0.009}$(syst.) ± 0.029(stat.)

Table 6.3: *Muon trigger scale factor as estimated for each of the ten $\eta - \phi$ bins. Numbers from [148].*

Similarly, the electron scale factor is also evaluated uniformly in η and ϕ range with a value of:

$$SF_{e,reco} = 1.000 \pm 0.015(stat. + syst.) \ . \tag{6.1.6}$$

For the identification however, the estimation is separated in different η areas and for different E_T ranges. Together with the identification, the isolation efficiency of electrons is measured. Detailed descriptions on the above measurements are documented in [148, 160]. The combined result of identification and isolation efficiencies is shown in table 6.4, separated in the different kinematic regions. Only very small fluctuations are observed in between $E_T - \eta$ regions.

	$SF_{e,id,iso}$			
	$\eta \in$			
E_T **(GeV)**	$[-2.47, 2.01]$	$[-2.01, -1.52]$	$[-1.37, -0.8]$	$[-0.8, 0]$
20-25	0.917 ± 0.082	0.946 ± 0.084	0.968 ± 0.083	0.907 ± 0.082
25-30	0.960 ± 0.028	0.990 ± 0.032	1.013 ± 0.029	0.949 ± 0.027
30-35	0.998 ± 0.027	1.029 ± 0.030	1.053 ± 0.027	0.987 ± 0.025
35-40	0.996 ± 0.024	1.027 ± 0.028	1.051 ± 0.025	0.985 ± 0.023
40-45	0.998 ± 0.025	1.029 ± 0.029	1.053 ± 0.026	0.987 ± 0.024
>45	1.007 ± 0.033	1.038 ± 0.037	1.062 ± 0.034	0.995 ± 0.032

	$SF_{e,id,iso}$			
	$\eta \in$			
E_T **(GeV)**	$[0, 0.8]$	$[0.8, 1.37]$	$[1.52, 2.01]$	$[2.01, 2.47]$
20-25	0.912 ± 0.082	0.970 ± 0.082	0.961 ± 0.086	0.953 ± 0.086
25-30	0.955 ± 0.027	1.016 ± 0.028	1.006 ± 0.038	0.998 ± 0.036
30-35	0.993 ± 0.025	1.056 ± 0.026	1.046 ± 0.037	1.037 ± 0.035
35-40	0.991 ± 0.023	1.054 ± 0.024	1.044 ± 0.035	1.035 ± 0.034
40-45	0.993 ± 0.024	1.056 ± 0.024	1.046 ± 0.036	1.037 ± 0.034
>45	1.002 ± 0.032	1.065 ± 0.033	1.055 ± 0.042	1.046 ± 0.041

Table 6.4: *Electron identification and isolation scale factors as estimated with respect to different η and E_T ranges. Numbers from [160].*

6.2 Simultaneous template fit method

A key element of the method we present here is that an extended dataset is utilized that includes also areas of the phase-space that are dominated by background events. In particular all events with at least three "good" jets with $p_{\mathrm{T}} \geq 25$ GeV are considered. This dataset is subsequently separated in four distinctive kinematic regions based on their overall jet multiplicity and the b-jet multiplicity, these regions have already been defined in section 4.5.1.

Compared to a cut-and-count method where Monte Carlo or data-driven background estimates would be subtracted by the collected data in a given signal region ,the fit approach we implement has two main advantages. Firstly, a higher-statistics sample is made available for the cross-section measurement by including background-dominated regions. Secondly, exactly because of the inclusion of these regions it is possible to parametrize the method in such a way that strong constraints can be placed to the background normalization. The information from background-dominated areas can subsequently be translated to the signal region.

In our method we first characterize independently the signal and the background contributions with functional templates that are obtained from the shape of their M_{jjj} distributions. We then perform an extended likelihood fit on the observed data simultaneously in all regions keeping the shape of the templates fixed and their relative normalization free to float.

Formulation

Mathematically, the method is described by a set of four equations, one for each of the kinematic regions that are of interest. The total number of events within each region is given by:

$$N_{obs}^{i,j} = \varepsilon_S^{i,j} N_S^i T_S^{i,j} + \varepsilon_B^{i,j} N_B^i T_B^{i,j} \ , \tag{6.2.1}$$

where the subscript S refers to signal and B to background events and the i and j superscripts denote the jet multiplicity ($i = 3$ or $i \geq 4$) and b-jet multiplicity ($j = 0$ or $j \geq 1$) respectively[1]. The parameters that appear in the formula are:

- The event tagging rate ($\varepsilon^{i,j}$) of the background or signal events in the i-th jet multiplicity and j-th b-jet multiplicity region.
- The template function ($T^{i,j}$), built from the shape of the M_{jjj} distribution for signal or background, at the i-th jet multiplicity and j-ith b-jet multiplicity region.
- The total number of signal or background events ($N_{S,B}^i$) in the i-th jet multiplicity region.
- The total number of observed events ($N_{obs}^{i,j}$) in the i-th jet multiplicity and j-ith b-jet multiplicity region.

These are described in greater detail in the following paragraphs and a summary is shown in table 6.6 at the end of this section.

6.2.1 Template Functions

The template functions are extracted by fitting the M_{jjj} distribution with a functional form. For the case of the background, the distribution is extracted in a data-driven way following the observations and the methodology presented in chapter 5. On the other hand the signal

[1]The $i = 3$ and $i \geq 4$ will also be referred to as 'three-jet' and 'four-jet' regions respectively. Similarly, the $j = 0$ and $j \geq 1$ will be referred to as the 'no-tag' and 'tagged' regions respectively, while for the case of $j \geq 0$ the term 'pre-tagged' is used.

templates are entirely taken from Monte Carlo. The following functional form is used to fit the background shapes:

$$f(x) = \begin{cases} \frac{\alpha}{\sqrt{2\pi}} e^{-\frac{(x-x_0)^2}{2\sigma^2}} & \text{, if } x < x_0 + \frac{1}{2\gamma}\sigma^2 \\ \frac{\beta}{\sqrt{2\pi}} e^{-\frac{(x-x_0)}{2\gamma}} & \text{, if } x \geq x_0 + \frac{1}{2\gamma}\sigma^2 \end{cases} , \tag{6.2.2}$$

which translates to a gaussian on the left-hand side of the M_{jjj} distribution and an exponential to the right-hand side. Parameters α and β define the normalization of the function, x_0 is the position of the peak of the distribution, σ is the width of the gaussian and γ is the inverse of the exponential falling rate. The left and right-hand side of the function are distinguished by a cross-over point (x_c) which is estimated by requiring the function to be continuous, hence the following must hold:

$$f(x = x_c)_{left} = f(x = x_c)_{right} \quad \text{, and}$$
$$\left.\frac{df_{left}}{dx}\right|_{x=x_c} = \left.\frac{df_{right}}{dx}\right|_{x=x_c} .$$

A direct consequence of this is that the normalization parameters in each part of the function are related by the following:

$$\beta = \alpha e^{\frac{\sigma^2}{8\gamma}} ,$$

therefore reducing the independent fit parameters by one. For the case of the signal templates, the above function is again used but with an additional gaussian introduced to the model. This extra gaussian parametrizes the expected top quark signal peak.

Figure 6.1 shows the fitted distributions of signal (first and third lines) and background (second and fourth lines) for the μ-channel (top two lines) and e-channel (bottom two lines) respectively. Once the parameters are determined, the template function is formed and is kept fixed in formula 6.2.1.

6.2.2 Event Tagging Rates

For each jet multiplicity region an efficiency parameter is defined that represents the number of signal (background) events with at least one "good" jet of $p_{\mathrm{T}} \geq 25$ GeV being identified as a b-jet (hence having a weight from the `SV0` tagger of at least 5.85) divided by the total number of signal (background) events in the given region. The following, thus, holds:

$$\varepsilon_X^{i,1} = \frac{N_X^{i,1}}{N_X^i} , \tag{6.2.3}$$

where X denotes either the signal (S) or background (B) events. This parameter is introduced in formula 6.2.1 as the event tagging rate and it holds by definition that $\varepsilon^{i,1} = 1 - \varepsilon^{i,0}$.

For the signal events the tagging rates ($\varepsilon_S^{4,1}$, $\varepsilon_S^{3,1}$) are determined from the Monte Carlo sample and are introduced in the fit as fixed parameters. On the other hand, the tagging rates for the background are introduced through $\varepsilon_B^{3,1}$ and a scale factor that translates the rate from the three-jet region to the four jet region ($SF_{3\to4}$), hence the following holds:

$$\varepsilon_B^{4,1} = SF_{3\to4}\varepsilon^{3,1} . \tag{6.2.4}$$

In this formulation the $SF_{3\to4}$ parameter is estimated from the Monte Carlo while the $\varepsilon^{3,1}$ term is free to float. We prefer the use of the scale factor, instead of just simply taking $\varepsilon_B^{4,1}$

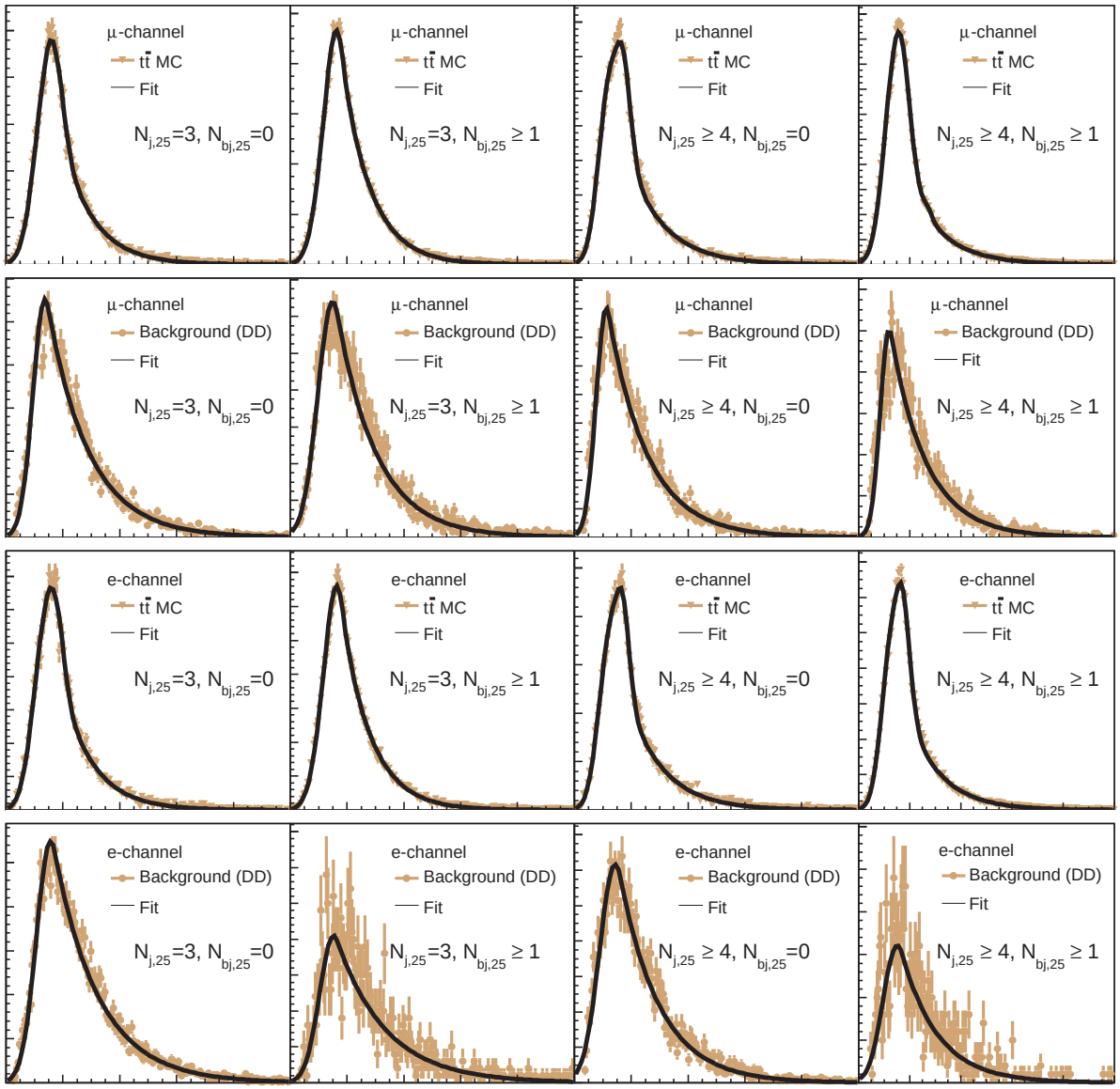

Figure 6.1: *Functional fit of M_{jjj} distributions: the x-axis corresponds to the value of M_{jjj} in the range [0,1000] GeV while the y-axis gives the normalization (number of events) which is not relevant for the extraction of the shape. The bin width is set at 5 GeV. In the first and second lines the μ-channel is shown, signal and background respectively, and in the third and fourth lines the e-channel, also signal and background respectively. The four columns correspond to the kinematic regions of interest, from left to right: $N_{j,25} = 3$ & $N_{bj,25} = 0$, $N_{j,25} = 3$ & $N_{bj,25} \geq 1$, $N_{j,25} \geq 4$ & $N_{bj,25} = 0$, $N_{j,25} \geq 4$ & $N_{bj,25} \geq 1$. The background distributions are all obtained using the data-driven method (see chapter 5) while the signal ones are taken from Monte Carlo.*

from Monte Carlo, because, as it is a ratio of the respective efficiencies, it is less sensitive in systematic effects.

In order to improve the fit method with respect to the expected systematic uncertainties on the background parametrization, a gaussian term on $\varepsilon^{3,1}$ is applied; this is explained in the next paragraph.

The constraint on $\varepsilon^{3,1}$

We define the following relation for the $\varepsilon^{3,1}$ term:

$$\varepsilon_B^{3,1} = \varepsilon_B^{2,1} SF_{2\to 3} \ , \tag{6.2.5}$$

where the $\varepsilon_B^{2,1}$ corresponds to the event tagging rate of background events at the exclusive two-jet bin, namely events with exactly two "good" jets of $p_{\mathrm{T}} \geq 25$ GeV, and the $SF_{2\to 3}$ is a factor that translates the rate of background events to the corresponding three-jet region, similar to the $SF_{3\to 4}$.

The $SF_{2\to 3}$ factor is entirely obtained from Monte Carlo. On the other hand, the $\varepsilon_B^{2,1}$ has the advantage that it corresponds to a kinematic region which is expected to be dominated by background events. Thus, it can be calculated from the observed data events with only requiring a correction for the expected signal contamination which is introduced from the Monte Carlo. It holds that :

$$\varepsilon_B^{2,1} = \frac{N_{obs}^{2,1} - N_{t\bar{t}}^{2,1}}{N_{obs}^{2} - N_{t\bar{t}}^{2}} \ , \tag{6.2.6}$$

where N_{obs}^2 and $N_{t\bar{t}}^2$ is the number of pre-tagged data and Monte Carlo $t\bar{t}$ events respectively, while $N_{obs}^{2,1}$ and $N_{t\bar{t}}^{2,1}$ is the subsets of events that are tagged. The corresponding yields for each channel are shown in table 6.5. The estimate of $\varepsilon_B^{2,1}$ now depends mainly on the available data statistics and the description of the signal events by the Monte Carlo which is substantially more accurate than the background estimates as it is simulated by a next-to-leading order generator.

Having calculated $\varepsilon_B^{2,1}$ from 6.2.6, the $\varepsilon^{3,1}$ enters the fit as gaussian constrained parameter with a central value that is obtained from equation 6.2.5 and with a width taken equal to the uncertainty that comes from the $\varepsilon_B^{2,1}$ term. The reason for this is to disentangle the uncertainty that is entirely Monte Carlo based, like in the case of the $SF_{2\to 3}$, as it will be taken into account for the calculation of the systematics later on. The uncertainty of $\varepsilon_B^{2,1}$ is driven by the data statistics and the description of the simulation which affects the acceptance of $t\bar{t}$ events (systematic). The systematic part is obtained by calculating the $t\bar{t}$ contribution for each of the variated Monte Carlo samples that are used for the systematic checks and comparing the value with the one from the reference Monte Carlo. Subsequently, all the deviations are added in quadrature and are combined with the statistical uncertainty giving a total of 17.8% for the e-channel and 14.9% for the μ-channel parameter.

6.2.3 Jet multiplicity ratio

In the template fit as described by 6.2.1, the parameters N_S^3, N_S^4, N_B^3 and N_B^4 are left free to float. They can be connected to the total number of signal or background events with the following relations:

$$\begin{aligned} N_X^3 &= \epsilon_X^3 N_X \text{ and similarly} \\ N_X^4 &= \epsilon_X^4 N_X \ , \end{aligned} \tag{6.2.7}$$

Parameter	μ-channel	e-channel
N^2_{obs}	4677	2534
$N^{2,1}_{obs}$	271	131
$N^2_{t\bar{t}}$	69.9	52.2
$N^{2,1}_{t\bar{t}}$	38.9	29.6

Table 6.5: *Event yields in the two-jet region for data (N^2_{obs}, $N^{2,1}_{obs}$) and $t\bar{t}$ Monte Carlo ($N^2_{t\bar{t}}$, $N^{2,1}_{t\bar{t}}$) events.*

where X refers to signal (S) or background (B) events and N_X is the total number of the given type of events. Similarly to the event tagging rates, the parameters ϵ^3_X and ϵ^4_X are defined as the rates of having three-jet or four-jet events of a given type, irrespectively of the content of b-tagged jets. We can parametrize these rates with in the following way:

$$\epsilon^3_X = \frac{1}{1+R_X} \text{ and} \tag{6.2.8}$$

$$\epsilon^4_X = \frac{R_X}{1+R_X} \ , \tag{6.2.9}$$

where R_X is the ratio of the number of four-jet events over the number of three-jet events, namely:

$$R_X = \frac{N^4_X}{N^3_X} \ . \tag{6.2.10}$$

The better description of the signal Monte Carlo events allows for the R_S parameter to be known with a better accuracy. Since we make no assumption on the total number of signal events we can take advantage of this and apply a gaussian constraint on R_S. The central value of the constrained parameter is obtained from Monte Carlo, while its deviation is calculated as the quadratic sum of all systematic variations and is taken as the width of the gaussian. The variations are obtained by comparing the value from the reference Monte Carlo with the value that is extracted by performing a fit with the R_S unconstrained on the variated Monte Carlo (pre-fit). The uncertainty estimate is 30.3% for the e-channel and 22.5% for the μ-channel. For the background events the relationship between N^3_B and N^4_B is also parametrized by R_B but no constrain is applied.

A summary of the parameters that are present in the fit is given in table 6.6.

6.3 Validation of the fit

We validate the fit method by applying it on the nominal Monte Carlo samples treating the latter as "data" (pseudo-data). Naturally, no data-driven approach is used and the parameters that are given as input correspond to an ideal description of the data by the Monte Carlo. This also includes the background templates, which should follow the data as they are obtained in a data-driven way, and therefore are re-computed from the combination of the Monte Carlo samples. The constrained parameters obtain their gaussian central values likewise and their width remains the same as shown in the previous section. Each of the fitted free parameters is compared using the relation:

$$\delta_x = \frac{x_{fit} - x_{input}}{x_{input}} \ ,$$

Fit Parameter	Type	Comments
$T_B^{3,0}, T_B^{3,1}, T_B^{4,0}, T_B^{4,1}$	Data-driven	Fixed shape templates. See chapter 5.
$T_S^{3,0}, T_S^{3,1}, T_S^{4,0}, T_S^{4,1}$	Monte Carlo	Fixed shape templates.
$\epsilon_S^{3,1}$, $\epsilon_S^{3,0}$	Monte Carlo	Constrained with $\epsilon_S^{3,0} = 1 - \epsilon_S^{3,1}$
$\epsilon_S^{4,1}$, $\epsilon_S^{4,0}$	Monte Carlo	Constrained with $\epsilon_S^{4,0} = 1 - \epsilon_S^{4,1}$
$\epsilon_B^{3,1}$, $\epsilon_B^{3,0}$	Gaussian constraint	Central value from $\epsilon_B^{3,1} = \epsilon^{2,1} SF_{2\to3}$, width from $\epsilon_B^{2,1}$ uncertainty. Constrained with $\epsilon_B^{3,0} = 1 - \epsilon_B^{3,1}$
$\epsilon_B^{4,1}$, $\epsilon_B^{4,0}$	Derived	$\epsilon_B^{4,1} = \epsilon^{3,1} SF_{3\to4}$. Connected with $\epsilon_B^{4,0} = 1 - \epsilon_B^{4,1}$,
$SF_{3\to4}$	Monte Carlo	
N_S^3, N_S^4	Free	Connected with $R_S = N_S^4/N_S^3$, R_S is constrained with a gaussian term.
N_B^3, N_B^4	Free	Connected with $R_B = N_B^4/N_B^3$, R_B is free.

Table 6.6: *List of the parameters that are involved in the fit (see equation 6.2.1).*

	μ-channel	e-channel
x	δ_x	
N_S	-0.0059	-0.0082
N_B	0.0005	0.0005
R_S	0.0083	0.0041
R_B	-0.0016	0.0013
$\epsilon_B^{3,1}$	0.0037	0.0087

Table 6.7: *Relative difference of fitted value versus input value for each of the floating parameters of the fit. The results are obtained from a single fit on the Monte Carlo samples (validation fit).*

where x_{input} is the true value of the parameter, which is also given as initial value to the fit, and x_{fit} is the resulting fitted value. The result of the validation fit is summarized in table 6.7 where it is shown that δ_x is very close to unity for all parameters, demonstrating a good behavior of the fit.

Ensemble test

In order to ensure that the fit is not biasing the result, we perform an ensemble test of 10000 pseudo-experiments (PSEs) for each channel. Each PSE is generated from the shape

of the expected distributions, it corresponds to an integrated luminosity of 35.3 pb^{-1} and the normalization of signal and background at each bin is randomized following Poisson statistics. Each PSE is subsequently fitted and the result of the fit is stored. We determine the bias on N_S and N_B by calculating their *pull* distributions, where the pull is defined as:

$$pull = \frac{N_{real} - N_{fit}}{\sigma_{fit}} \ , \tag{6.3.1}$$

where N_{real} is the number of the generated number of events, N_{fit} is the number of events that the fit estimates and σ_{fit} is the uncertainty that is returned by the fit. A standard normal distribution is expected and therefore the resulting pulls are fitted with a gaussian function. In case the mean of the gaussian is larger (smaller) than zero, a negative (positive) bias is observed. Figures 6.2(a) and 6.2(b) show the results of the pulls for the μ-channel and the e-channel respectively and in all cases the resulting gaussian parameters are within expectations.

Linearity test

As a last check we perform a linearity test for different input cross-sections. We create variations of the Monte Carlo samples where the signal is re-weighted such that it corresponds to the different cross-sections, starting from 120 pb. up to and including 220 pb. in steps of 10 pb. The background samples remain the same. As before, we perform an initial fit and subsequently 2000 PSEs are drawn for each variation of the Monte Carlo. The resulting N_S are then fitted with a gaussian function and the mean is used to evaluate the fitted cross-section.

The sigma of the gaussian is divided by the square root of the total number of PSEs and is used as the error on the estimate. Figure 6.2(c) shows the estimated cross-section with respect to the input cross-section. A first degree polynomial of the form $y = \alpha + \beta x$ is used to fit the points and, as expected, the y-intercept point α is close to zero and the slope parameter β close to one; this is consistent in both channels.

6.4 Application on Data

Following the description given in section 6.2, we give as input to the fit the M_{jjj} template shapes (as calculated in section 6.2.1), the parameters that are taken from the Monte Carlo and are kept fixed (namely the signal tagging rates and the background scaling factor $SF_{3\to4}$), and lastly the constrained gaussian terms. Table 6.8 summarizes the values of these parameters.

The resulting M_{jjj} distributions from the fit are shown in figure 6.3 for the μ-channel and in figure 6.4 for the e-channel. The number of signal and background events that is estimated from the fit is shown in table 6.9. The quoted uncertainty is statistical and is obtained by performing 2000 PSEs; the relevant distributions for the number of signal events are shown in figure 6.5.

It is evident that the agreement of the fits to the data is very good for all the kinematic regions defined and for both channels. As expected, the 3-jet and 4-jet regions are completely dominated by background in the no-tag bin, while in their tagged bins it is considerably reduced. This highlights the importance of b-tagging for selecting signal events. The apparent difference in the yield of background between muon and electron channel is due to the different cuts applied in the two channels, namely with respect to the selection based on $E_{\mathrm{T}}^{\mathrm{miss}}$ and $M_{W,T}$ cuts.

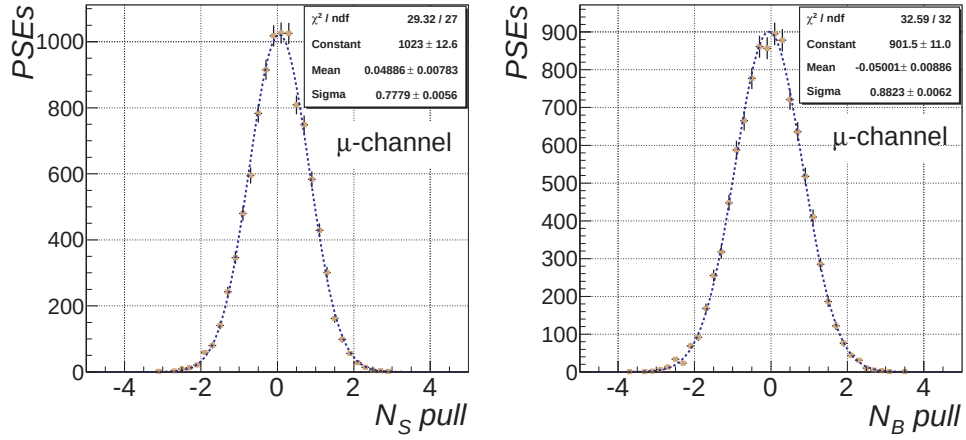

(a) *μ-channel: N_S (left) and N_B (right) pull distributions.*

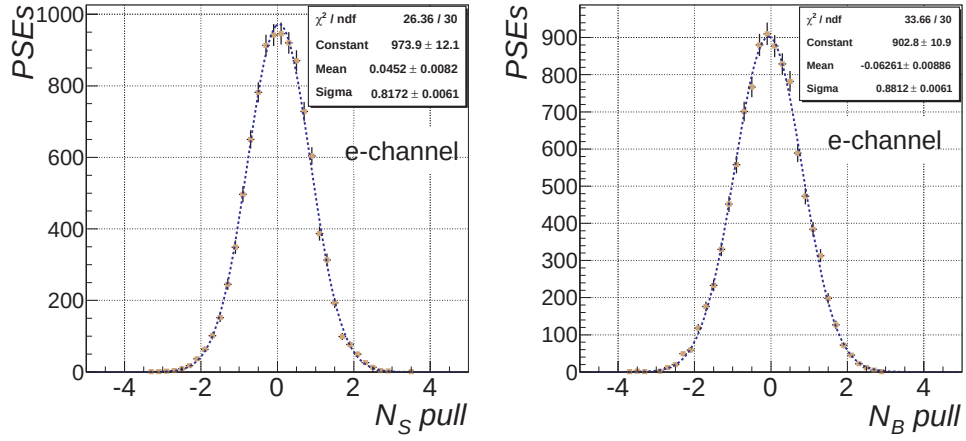

(b) *e-channel: N_S (left) and N_B (right) pull distributions.*

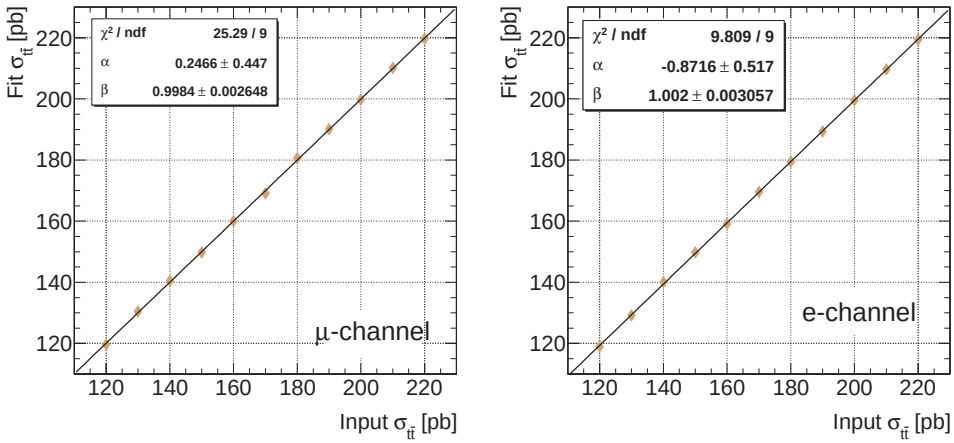

(c) *Linearity test for μ-channel (left) and for e-channel (right)*

Figure 6.2: *The pull distributions of N_S and N_B, drawn from an ensemble test of 10000 PSEs, are shown for the μ-channel (a) and for the e-channel (b). In addition, the linearity test performed for different input signal cross-sections is shown in (c) for both channels: the μ-channel (left) and the e-channel (right). The points from the linearity test are fitted with a first degree polynomial.*

	μ-channel		e-channel	
	Values of Monte Carlo fixed terms			
$\varepsilon_S^{3,1}$	0.6603		0.6668	
$\varepsilon_S^{4,1}$	0.7321		0.7273	
$SF_{3\to4}$	1.6699		1.7895	
	Gaussian-constrained terms			
	Value	**Uncertainty**	**Value**	**Uncertainty**
$\varepsilon_B^{3,1}$	0.0918	±0.0137	0.0700	±0.0125
R_S	1.6792	±0.3778	1.6405	±0.4971

Table 6.8: *Input values of parameters that are given as input to the fit. The $\varepsilon_S^{3,1}$, $\varepsilon_S^{4,1}$ and $SF_{3\to4}$ are kept fixed while $\varepsilon_B^{3,1}$ and R_S are given as gaussian constraints. A detailed description is given in sections 6.2.2 and 6.2.3.*

	μ-channel	e-channel
N_S	386.9 ± 35.7	392.1 ± 55.8
N_B	1451.1 ± 48.1	769.0 ± 59.7

Table 6.9: *Number of signal and background events as calculated by applying the simultaneous template fit on the 35.3 pb^{-1} of $\sqrt{s} = 7$ TeV proton-proton collision data. The uncertainties are statistical and estimated from running 2000 PSEs.*

6.5 Systematic uncertainties

This section discusses the various sources of systematic uncertainties (systematics) that need to be taken into account in our cross-section calculation. The method we mainly follow depends on comparing the nominal Monte Carlo result with the result from variated versions of the simulation. The variation depends on the evaluated systematic source and typically corresponds to $\pm1\sigma$ uncertainty. We re-run the fit for each systematic check treating the variated samples as pseudo-data. It should be noted that the advantage of obtaining the background shape with a data-driven way is apparent now since we do not need to take it into account as a source of uncertainty. Therefore, for each systematic variation we re-evaluate the background templates based on the pseudo-data background distributions.

In the following, the Monte Carlo samples assume a top quark mass equal to 172.5 GeV. This choice is consistent with the current world average [53] but we do not assign a systematic for it. The reason is that for small deviations around this value the cross-section is expected to behave linearly. Likewise, we make an assumption for the branching ratio used in equation 6.0.1. We use the value of $BR = 0.543$, which is extracted as describe in the beginning of this chapter, and we conventionally assign no uncertainty to it. In fact, the contribution of the uncertainty is $< 1\%$ [53].

6.5.1 Lepton trigger, reconstruction and identification

The data-driven estimates of efficiencies, and consequently their scale factors, are not free from uncertainties and as a result they must be propagated to the final cross-section result. The values of the scale factor together with their uncertainties were already shown in section 6.1. It should be mentioned that because some scale factors are given with respect to kinematic

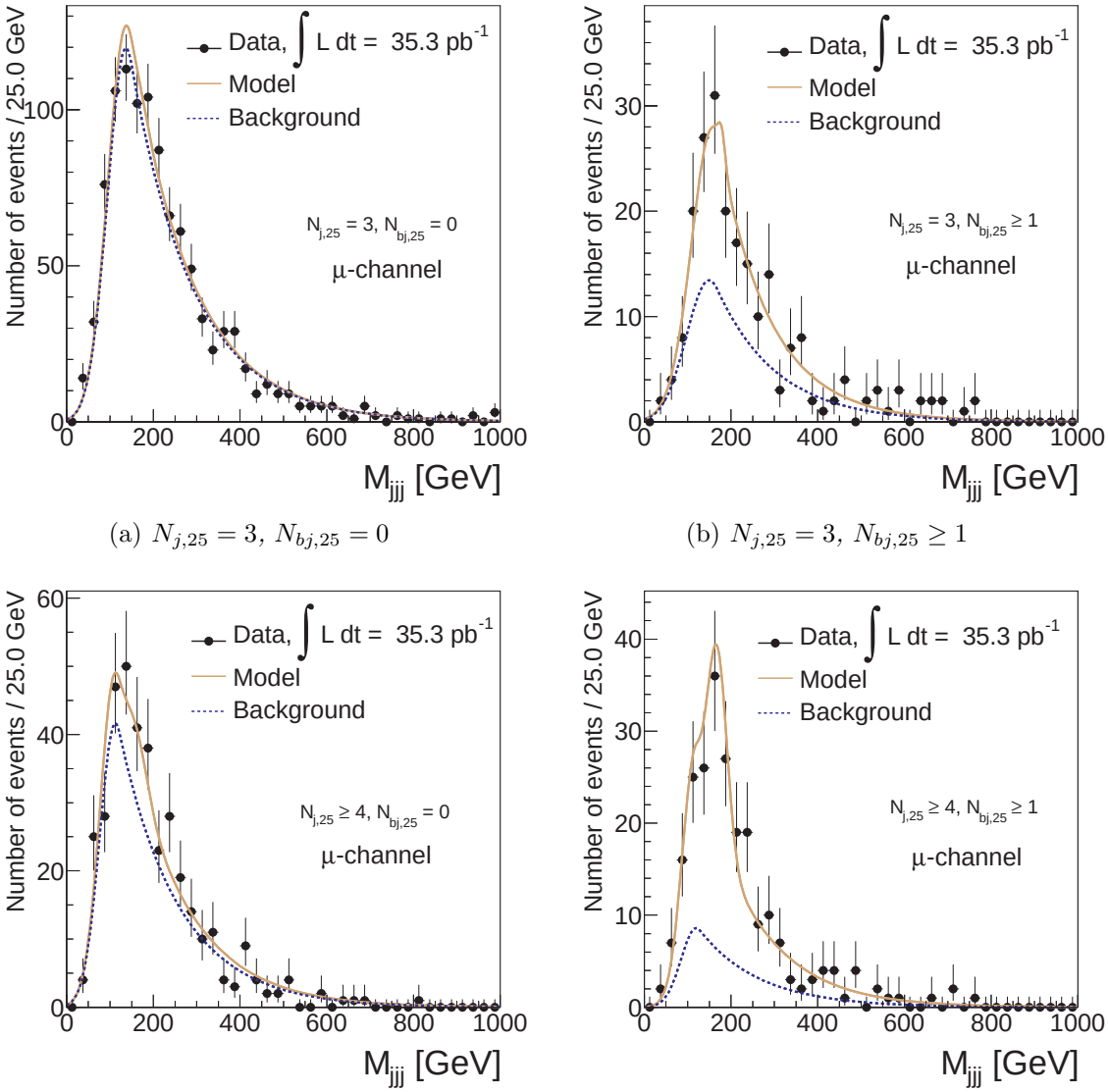

(a) $N_{j,25} = 3$, $N_{bj,25} = 0$

(b) $N_{j,25} = 3$, $N_{bj,25} \geq 1$

(c) $N_{j,25} \geq 4$, $N_{bj,25} = 0$

(d) $N_{j,25} \geq 4$, $N_{bj,25} \geq 1$

Figure 6.3: *The M_{jjj} distributions after applying the simultaneous template fit on the 35.3 pb^{-1} of $\sqrt{s} = 7$ TeV proton-proton collision data. The single-lepton top quark pair μ-channel selection is applied (section 4.4.3).*

ranges, they are not applied directly on the cross-section formula (equation 6.0.1) but are rather given as weights, event by event, depending on the kinematics of the identified lepton. The systematic variations are treated in a similar way by adjusting the weight accordingly.

The uncertainty on our analysis is evaluated by re-running the fit model on the variated Monte Carlo and comparing the results with the nominal case. Since these systematics are not expected to alter the shape of the backgrounds but only their acceptance, the background templates do not need to be re-evaluated. We find a modest 4% uncertainty for the e-channel and 1.5% for the μ-channel. The result is symmetrical in positive and negative deviations since almost all of the scale factors are given with a symmetrical uncertainty.

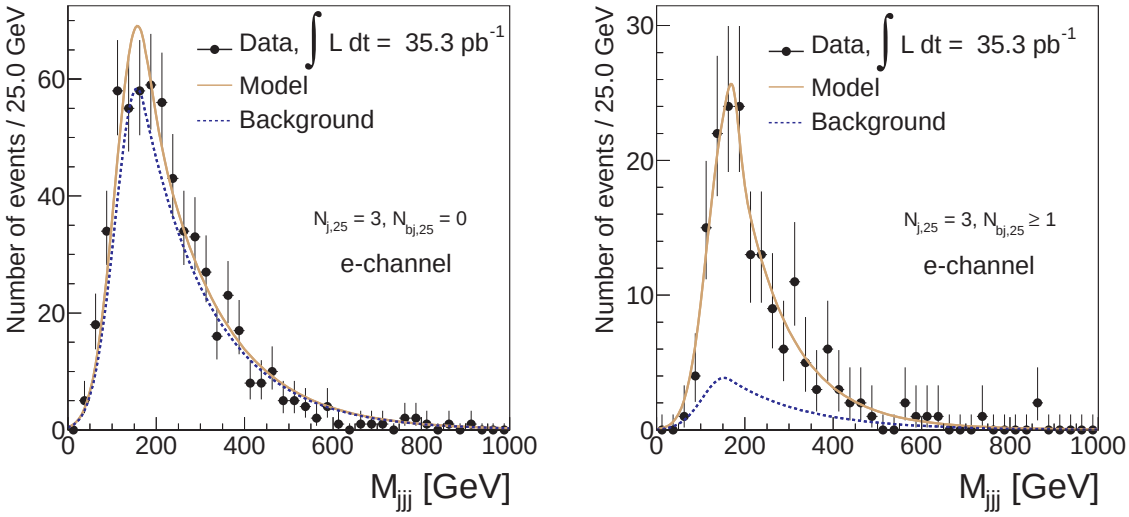

(a) $N_{j,25} = 3,\ N_{bj,25} = 0$

(b) $N_{j,25} = 3,\ N_{bj,25} \geq 1$

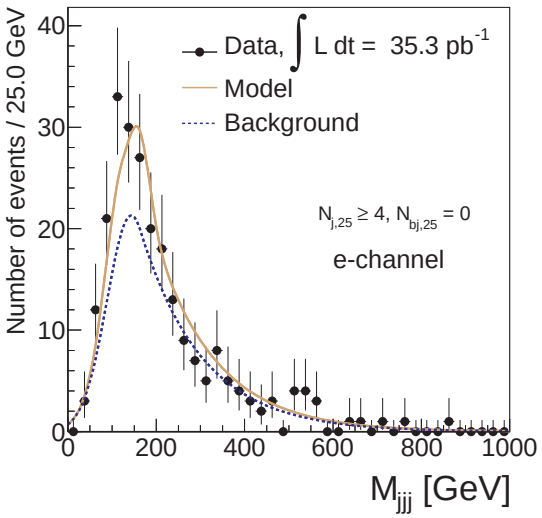

(c) $N_{j,25} \geq 4,\ N_{bj,25} = 0$

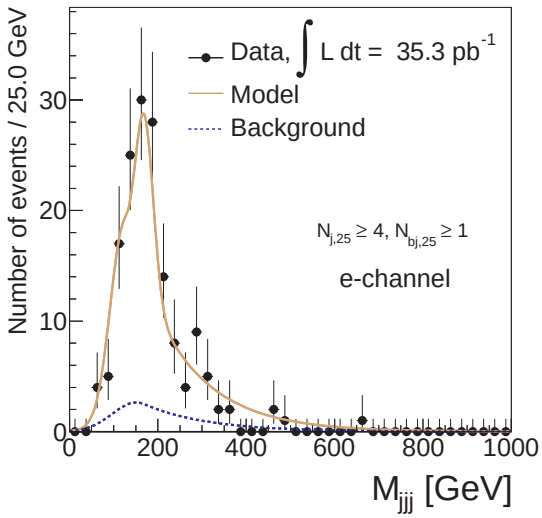

(d) $N_{j,25} \geq 4,\ N_{bj,25} \geq 1$

Figure 6.4: *The M_{jjj} distributions after applying the simultaneous template fit on the 35.3 pb^{-1} of $\sqrt{s} = 7$ TeV proton-proton collision data. The single-lepton top quark pair e-channel selection is applied (section 4.4.3).*

6.5.2 Lepton energy scaling and resolution smearing

In sections 4.2.1 and 4.2.2 the correction factors that are applied on the electrons and muons respectively for improving the agreement between Monte Carlo and data were given. For both muons and electron the energy scaling and resolution is applied by default on the nominal Monte Carlo but naturally their related uncertainties must be taken into account. The implementation is similar as before where the correction factors are given as a weight on event by event and their uncertainties are accounted by adjusting the weight. Likewise, the estimation of the final uncertainty on the cross-section is obtained by comparing the nominal Monte Carlo with their variated versions. We find that for the electron channel the contribution is relatively small at about $+1.3/-1.2\%$ and even smaller for the muon channel, at $\pm 0.4\%$.

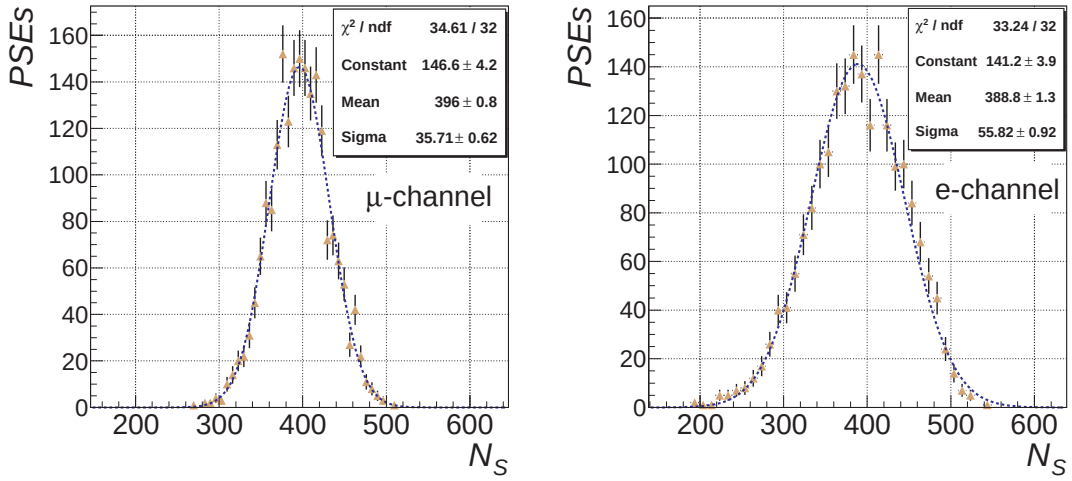

(a) *μ-channel* (b) *e-channel*

Figure 6.5: *Distributions of N_S from 2000 PSEs ran after the fit to the data. The fitted gaussian sigma is taken as the statistical uncertainty on the signal events.*

6.5.3 Jet energy scale

One of the uncertainties that is expected to be more prominent comes from the jet energy scale corrections (JES). The various sources of uncertainty on the JES are estimated from a combination of in-situ measurements of the single hadron response, either from data or pion test-beam measurement, and systematic variations of Monte Carlo samples. The total uncertainty is given per jet depending on its transverse momentum and pseudo-rapidity. The following systematic sources are considered:

- Detector effects such as distortions and un-instrumented material which are evaluated by testing different geometry models.
- The calorimeter cluster noise for topological clusters which is varied with a ±10%.
- The Monte Carlo modeling used in event generation.
- The "non-closure" of the jet calibration step (see section 4.1.3).
- Effects from multiple interaction within one event (pile-up).

The result of each particular source are documented in detail in [161, 162]. For isolated jets reconstructed with the `anti-`$k_\perp$ and with $R = 0.4$, and calibrated with the `EMJES` scheme, the JES systematic uncertainty as a function of p_{T} and η is shown in table 6.10. To the above calculations a conservative approach is taken for accounting close-by activity by adding 5% to each jet for when a second jet with $p_{\mathrm{T}} > 10$ GeV resides within $\Delta R \leq 0.6$ [163].

In this analysis, each jet in the Monte Carlo is varied by its 1σ variation, upwards or downwards, creating two different samples. After running the fit on the two variations we compare their results with the one obtained from the nominal case. The uncertainty we find for the *e*-channel is considerably high at $+5.3/-6.2\%$ and slightly lower for the μ-channel at $+4.2/-5.8\%$.

η region	Maximum fractional JES uncertainty		
	$p_T^{jet} = 20$ GeV	$p_T^{jet} = 200$ GeV	$p_T^{jet} = 1.5$ TeV
$0.0 < \|\eta\| < 0.3$	4.1%	2.3%	3.1%
$0.3 < \|\eta\| < 0.8$	4.3%	2.4%	3.3%
$0.8 < \|\eta\| < 1.2$	4.3%	2.5%	3.5%
$1.2 < \|\eta\| < 2.1$	5.2%	2.6%	3.6%
$2.1 < \|\eta\| < 2.8$	8.2%	2.9%	
$2.8 < \|\eta\| < 3.2$	10.1%	3.5%	
$3.2 < \|\eta\| < 3.6$	10.3%	3.7%	
$3.6 < \|\eta\| < 4.5$	13.8%	5.3%	

Table 6.10: *The maximum JES systematic uncertainties for isolated jets, reconstructed with* `anti-`$k_\perp$ *(R=0.4) and calibrated with* `EMJES`*, as estimated from Monte Carlo. Numbers taken from [162].*

6.5.4 Jet energy resolution

In section 4.2.3 the jet energy resolution (JER) correction was discussed. The smearing is applied by default on the nominal Monte Carlo in order to improve the agreement with the data. Running the fit model on the smeared sample, which is used as the reference sample throughout the analysis, we compare the result with the one from the non-smeared simulation. This is taken as the systematic uncertainty due to the JER corrections and it amounts to $\pm 1.9\%$ for the e-channel and $\pm 1.8\%$ for the μ-channel.

6.5.5 Jet reconstruction efficiency

In a similar way as with the lepton reconstruction efficiency, the jet reconstruction efficiency is defined ($\epsilon_{jet,reco}$). The $\epsilon_{jet,reco}$ is measured for calorimeter jets, which are used in this analysis, with respect to track jets, namely jets that are built solely from charged particle track information obtained by the Inner Detector; track jet reconstruction and performance is documented in [164]. The method typically relies on matching a jet, which is identified in the calorimeters, with a jet reconstructed at the Inner Detector. Since the two reconstruction methods depend on different techniques, due to the different input parameters, they also have different systematic sources allowing for complementarity.

For the jets used in our analysis (`anti-`$k_\perp$), both Monte Carlo and data samples are used in order to extract the $\epsilon_{reco,jet}$. Comparison between them shows very small differences and within the uncertainty limits, especially for calorimeter jets with $p_{\mathrm{T}} \geq 20$ GeV, hence no scale factor is assigned [165]. For the uncertainty a conservative approach is followed where the 2%, at maximum, residual difference between data and Monte Carlo is propagated to our calculation. This is implemented by randomly rejecting a 2% of jets and comparing the fit result with respect to the nominal Monte Carlo. We find that the cross-section result deviates by $\pm 2.8\%$ and $\pm 3.3\%$ for the e-channel and μ-channel respectively.

6.5.6 b-tagging calibration

Section 4.2.5 discussed the corrections applied to the jets with respect to the b-jet identification. The respective scale factors are applied by default on a jet-by-jet basis in the form of event weights; they are shown in tables 4.3. Similarly to the corrections for the leptons and the

jet resolution smearing, the corresponding uncertainties need to be propagated to the final analysis. We take the $\pm 1\sigma$ variations of the scale factors to obtain the upward and the downward fluctuations. We compare the fit result from the variated samples with the one from the nominal Monte Carlo and we obtain the respective uncertainty. The uncertainty is found to be considerable, at $+3.3/-4.9\%$ for the electron channel and $+3.5/-4.2\%$ for the muon channel.

6.5.7 Heavy flavor composition in W+jets events

The composition of W+jets from b-jets, c-jets or light jets can be an important source of uncertainty as it can affect the value of the event tagging rates and as a consequence the parameters $SF_{2\to3}$ and $SF_{3\to4}$ which are used in the fit.

The Monte Carlo is corrected at the exclusive two-jet bin for its $Wb\bar{b}$ and $Wc\bar{c}$ fractions. This correction is associated with a 50% uncertainty for the $Wb\bar{b}$ and $Wc\bar{c}$, fully correlated between the two processes. In addition, a 40% uncertainty is associated to the uncorrected Wc fraction. These uncertainties are derived according to the data-driven method as documented in [152]. For extrapolating from the two-jet bin to the three-jet and four-jet bin we use a conservative approach based on results from Monte Carlo studies and therefore an additional 20% per bin is linearly added for all cases. The $Wb\bar{b}$ and $Wc\bar{c}$ are again taken as fully correlated. The final result of the uncertainty is found to be particularly large with $+5.5/-5.8\%$ at the e-channel and $+7.5/-5.8\%$ at the μ-channel.

6.5.8 Normalization of the background

The normalization of the background becomes an input to the fit through the use of the $SF_{2\to3}$ and $SF_{3\to4}$ scale factors, where the first enters via the constrained parameter $\varepsilon_B^{3,1}$ and the second is estimated from Monte Carlo and remains fixed. Since these parameters are ratios of event tagging rates we do not expect large variation due to the overall normalization of the background, nevertheless we still test the dependence for the QCD normalization and the sum of the rest of the backgrounds (except the W+jets).

QCD normalization

As mentioned in section 4.5.2 we do not rely on the Monte Carlo samples for QCD estimates but we use the event numbers as obtained from the data-driven methods documented in [159]. These numbers are extracted also per kinematic region and with respect to the number of b-tagged jets, therefore accounting for knowledge on heavy flavor composition. The data-driven results are given in table 4.10 along with their uncertainties. The uncertainties are propagated to our analysis by varying the Monte Carlo samples accordingly and, as before, comparing the fit result with the one from the nominal Monte Carlo. We find that the electron channel deviates at $+1.4/-0.6\%$ while the muon channel at only $+0.3/-0.1\%$, indeed a very small contribution.

Other backgrounds

Other contributing backgrounds are the single-top, the di-bosons and the Z+jets. Their normalization is taken from the respective Monte Carlo samples and therefore any uncertainty involved should be related with their theoretical prediction. For the Z+jets a conservative approach of variating the normalization by 100% is used. This takes into account the uncertainty with respect to the jet multiplicity as well as the heavy flavor content. For the

di-bosons a variation of 5% is taken, motivated by the theoretical uncertainty on the generator cross-section [166]. Similarly, the single-top is variated by 10% to account for the expected theoretical uncertainty [167]. The combined uncertainty for both channels is found to be very small, at the order of 0.1% and therefore omitted from the calculation.

6.5.9 Template systematics

Systematics from data-driven method

We should account for systematics that originate from the template parametrization. First we consider the data-driven method for the background templates. As discussed in section 5.2.2, the Monte Carlo comparison of the background shapes obtained after the baseline $t\bar{t}$ cuts and the QCD-enhancing cuts have a good agreement. We account for the possibility of mismodeling by comparing the nominal fit result, taken after applying the QCD-enhancing cuts on the data, with the fit result after using background templates that are derived from Monte Carlo; we perform the comparison with both `AlpGen` generated and `Sherpa` generated W+jets samples and we take the maximum deviation as the uncertainty. The final result, which is symmetrized, is $\pm 4.1\%$ and $\pm 3.5\%$ for the electron and the muon channels respectively.

Systematic from functional parametrization

In addition, as discussed in section 6.2.1 the template functions are obtained by doing a binned fit of the distributions with the function as given in equation 6.2.2. Naturally, the cross-section calculation is incurred by the choice of the functional form and the bin-size selected for the fit. We test the dependence on the functional form by substituting the function templates with binned templates obtained directly from the histograms and we re-run the fit comparing the result with the one from the nominal case. For the bin-size we re-calculate the templates with three different bin sizes, 1 GeV/*bin*, 5 GeV/*bin* and 20 GeV/*bin* and we take the 5 GeV/*bin* as our nominal case. We perform the fit for each version of the templates and we take the maximum deviation from the nominal case as the uncertainty. The two uncertainties are eventually added in quadrature and we find that the overall uncertainty is $\pm 1.2\%$ for either of the two channels.

6.5.10 Initial and final state radiation

An important source of uncertainty comes from the modeling of the initial and final state radiation (ISR and FSR respectively) of the signal Monte Carlo. The ISR/FSR parameters affect significantly the acceptance of the signal as they alter the jet multiplicity as well as the jet transverse momentum.

For the analysis presented here, the ISR and FSR uncertainty is determined by varying the relevant parameters of the underlying event tuning, such as the momentum scale, the Λ_{QCD} and the parton radiation cut-off mass. We use a leading-order signal simulation, the `AcerMC`, combined with `Pythia` for which six variated samples exist: maximum ISR, maximum FSR, minimum ISR, minimum FSR, maximum ISR and FSR, and minimum ISR and FSR. We run the fit on the nominal `AcerMC` signal, after re-evaluating the signal templates, and then we compare the result with all of the above variations. The final uncertainty is taken from the maximum positive and the maximum negative difference. We find a significant contribution of $+3.8/-4.8\%$ at the electron channels and of $+4.3/-5.2\%$ at the muon channel.

It should be noted that we do not use a next-to-leading order signal variation. The reason is that no final recommendation exists within ATLAS on how to vary ISR and FSR on next-

to-leading order generators.

6.5.11 Parton distribution functions

The choice of a Parton Distribution Function (PDF) for the event generation of the Monte Carlo gives rise to another source of uncertainty. For the analysis presented in this thesis the signal is produced using the CTEQ6.6 PDF while other samples are produced using MSTW08 [48] and NNPDF2.0 [168]. The treatment of the uncertainties follows the recommendations as reported by the PDF4LHC working group, documented in [169]. In principle, the uncertainty is evaluated for each of the three PDFs and for which error PDF sets exist. The error PDF sets have their PDF parameters varied upwards or downwards. For CTEQ exist 44 sets while for MWST are 42 and 100 for the NNPDF. The analysis must be repeated for each of those PDF. Practically, the samples are not re-generated with new PDFs but are re-weighted using the following:

$$w = \frac{P_{var}(x_1, f_1, Q) \cdot P_{var}(x_2, f_2, Q)}{P_{nom}(x_1, f_1, Q) \cdot P_{nom}(x_2, f_2, Q)} \ , \tag{6.5.1}$$

where P_{var} and P_{nom} are the variated and the nominal PDF set respectively, f_1 and f_2 are the flavors of the scattering partons while x_1 and x_2 are their fractional momenta. Finally, Q is the momentum transfer in the event.

The total uncertainty for each PDF family is obtained in the following way: for the CTEQ variations by using a symmetric Hessian calculation, for the MWST an asymmetric Hessian calculation and for the NNPDF is taken as the standard deviation of the variations. The final uncertainty is the linear combination of the three families. The PDF uncertainty affects mainly the acceptance of the events and the change on the template shapes is expected to be negligible. The result gives $\pm 1.7\%$ deviation for each of the two channels.

6.5.12 Signal generator, parton shower and fragmentation modeling

To test the dependance of the fit on the choice of the signal next-to-leading order simulation, we compare the result of the nominal Monte Carlo validation fit, which uses the `MC@NLO` event generator coupled with `HERWIG` for the hadronization, with the result obtained by using the `POWHEG` event generator using the same hadronization model. The found result yields a $\pm 2.6\%$ uncertainty for the e-channel and a $\pm 1.7\%$ uncertainty for the μ-channel.

In addition, we test the dependance on the hadronization model by comparing the result from using the `POWHEG/HERWIG` signal sample with the one estimated from using the `POWHEG/Pythia` version. In this case, since the first is taken as the nominal Monte Carlo the signal templates must be re-calculated accordingly. We find $\pm 1.2\%$ for the e-channel and $\pm 0.3\%$ for the μ-channel.

6.5.13 Multiple interaction activity (pile-up)

In our analysis we use the Monte Carlo samples without correcting for the pile-up activity to match the one seen from data. We account for this by assigning a systematic in the following way. We create a separate version of Monte Carlo samples in which the events are re-weighted such that they match the data expectation. The weight is applied on event-by-event basis according to the number of vertices with at least 5 tracks associated to each of them. It applies for all events in either the μ-channel or e-channel with at least three "good" jets with $p_{\mathrm{T}} \geq 25$ GeV. The relevant value of the weight is seen in table 6.11 and are obtained from [170].

Number of vertices	Weight
1	1.9290
2	1.3025
3	0.8380
4	0.6225
5	0.4635
≥ 6	0.4345

Table 6.11: *Weight applied on the Monte Carlo variation for pile-up systematic estimation. The value of the weight depends on the number of vertices that are found in the simulated event and have more than 5 tracks associated with them. Numbers taken from [170].*

The result of the fit from the nominal Monte Carlo is compared with the one taken from the variated samples and the final uncertainty is extracted. A considerable contribution of $\pm 5.8\%$ for the electron channel and $\pm 5.5\%$ for the muon channel is found.

6.5.14 Luminosity

The uncertainty on the luminosity is taken to be 3.4% and is based on the selected sample as already discussed in section 4.4.1. This value is obtained from [156] and the major contribution comes from the bunch charge product $n_1 \cdot n_2$, where n_1 and n_2 are the proton population in the colliding bunch of beam 1 (clockwise) and beam 2 (anti-clockwise) respectively. We translate this uncertainty to the cross-section uncertainty by varying it accordingly in equation 6.0.1.

6.6 Combination of channels

The events selected with the $t\bar{t}$ baseline selection are completely orthogonal between the electron and the muon channel; this is ensured by the charged lepton requirement, as explained in section 4.4.3. It is trivial, therefore, to combine the two channels into a single fit and take advantage from a higher statistics sample. In addition, we can obtain a single result for our analysis which can simplify the comparison with other methods that estimate the $t\bar{t}$ production cross-section.

In principle, the merging of the two channels can be achieved by simply selecting events and substituting the charged lepton requirement in one channel with the logical `OR` of the two charged lepton requirements. This would provide a single dataset from which we can estimate the signal templates as well as the values of the parameters that enter the fit, both those that are fixed from Monte Carlo and those that are constrained. However, the templates would need to be re-calculated. Specifically, an adjustment on the QCD-enhancing cuts for the extraction of the background shape is required, as well as additional validation of the method, which may increase the complexity of the method. Therefore, we do not follow this approach.

The method we use is to form a single likelihood from the two independent likelihoods of each channel, effectively using a total of eight distinct kinematic regions. The parameters for each channel remain the same, hence their respective initial values as well as the templates can be kept the same as for the individual channel fits. The total number of signal events can

now be parametrized in the following way:

$$N_{S,e} = \varepsilon_{S,e} N_S \text{ and}$$
$$N_{S,\mu} = \varepsilon_{S,\mu} N_S \ , \tag{6.6.1}$$

where $\varepsilon_{S,e}$ and $\varepsilon_{S,\mu}$ correspond to the selection efficiency for each channel with respect to the total signal events obtained from their combination, hence $N_{S,e}$ and $N_{S,\mu}$ is the signal events found in each channel. In a similar way to what happen in section 6.2.3 the efficiencies can be written as follows:

$$\varepsilon_{S,e} = \frac{RC_S}{1 + RC_S} \text{ and} \tag{6.6.2}$$
$$\varepsilon_{S,\mu} = \frac{1}{1 + RC_S} \ , \tag{6.6.3}$$

where RC_S is the ratio of the number of signal events found by the e-channel likelihood over the number of signal events found by the μ-channel likelihood. Thus:

$$RC_S = \frac{N_{S,e}}{N_{S,\mu}} \ . \tag{6.6.4}$$

For the fit the RC_S is left free to float. In the same way as described above we define RC_B as the ratio on the number of background events found by each channel. The RC_B is also left free to float.

The calculation of the cross-section from the extracted number of signal events is the same as given in equation 6.0.1 with all but the $t\bar{t}$ selection efficiency parameter ($\epsilon_{t\bar{t}}$) remaining the same. The latter now corresponds to the following:

$$\epsilon_{t\bar{t}} = \epsilon^{e}_{t\bar{t}} + \epsilon^{\mu}_{t\bar{t}} \ , \tag{6.6.5}$$

where $\epsilon^{e}_{t\bar{t}}$ and $\epsilon^{\mu}_{t\bar{t}}$ are the $t\bar{t}$ selection efficiencies for each individual channel. Because the selection cuts between the two channels are mutually exclusive, it is ensured that $\epsilon^{e}_{t\bar{t}} + \epsilon^{\mu}_{t\bar{t}} \leq 1$, since in the opposite case it would be unphysical. The additional advantage of this approach is that there is no need to re-calculate the scale factors, presented in section 6.1, for the trigger and the lepton reconstruction and identification.

The application of the above methodology on the data yields the result that is shown in table 6.12. After the combination of the channels, the treatment of the systematics can be done in the same way as presented in section 6.5.

	Channel combination
N_S	782.1 ± 59.6
N_B	2216.9 ± 68.0

Table 6.12: *Number of signal and background events as calculated by applying the channel-combined simultaneous template fit on the the 35.3 pb^{-1} of $\sqrt{s} = 7$ TeV proton-proton collision data. The uncertainties are statistical and estimated from running 2000 PSEs.*

6.7 Summary and discussion

The methodology for extracting the $t\bar{t}$ production cross-section was presented, including the explanation for the treatment of systematics. Thus far, the result of the fitted signal events

was shown in table 6.9 (section 6.4) for the fit on the individual channels and in table 6.12 (section 6.6) for the channel combination fit.

From the extracted number of signal events we can use equation 6.0.1. The total luminosity, already discussed in section 4.4.1, is 35.3 pb^{-1} and the branching ratio for normalizing to the total $t\bar{t}$ cross-section is taken as $BR = 0.543$ [53]. The $t\bar{t}$ signal efficiency before the scale factor corrections are shown in table 6.1 (section 6.1) for the respective kinematic regions. Combining them on an event-by-event basis with the scale factors shown in sections 6.1.1 and 6.1.2 we obtain an efficiency of 9.76% for the e-channel and of 13.15% for the μ-channel. The final result of the cross-section measurement using the simultaneous template fit method is shown in table 6.13 for the individual channel fits and their combination. The uncertainties that are taken into account are summarized in table 6.14.

	$t\bar{t}$ **cross-section,** $\sigma_{t\bar{t}}$ (pb)
e**-channel**	$209.6 \pm 29.8(stat.)^{+27.9}_{-30.4}(syst.)^{+7.3}_{-6.9}(lumi.)$
μ**-channel**	$153.5 \pm 14.1(stat.)^{+20.1}_{-20.6}(syst.)^{+5.4}_{-5.1}(lumi.)$
Combination	$178.1 \pm 13.5(stat.)^{+23.0}_{-24.6}(syst.)^{+6.2}_{-5.9}(lumi.)$

Table 6.13: *The $t\bar{t}$ cross-section from proton-proton collisions delivered by the LHC at $\sqrt{s} = 7$ TeV as estimated from the simultaneous template fit method on a total of 35.3 pb^{-1} dataset, corresponding to the 2010 ATLAS recorded dataset.*

With the measurement presented here a test of QCD is provided at an energy regime that was previously unexplored. Figure 6.6 shows the measurement made in this thesis in comparison with the theoretical expectations at NLO and (approximated) NNLO as estimated for a top quark mass of 172.5 GeV using the tool documented in [171]. Measurements from the Tevatron experiments, DØ and CDF, have shown at lower center-of-mass energies the good agreement between theory and experiment [172, 173, 174, 175]. It is evident that a good agreement with the theory is observed well within the limits of the estimated uncertainties.

Discussion

The analysis presented in this thesis covers an important milestone for the experiment. Not only it shows the great ability of the detector in identifying complex topologies in an immense background but it also illustrates that even with a small amount of data such measurements can be made with an acceptable total uncertainty. The method employed here, takes advantage of a greater kinematic region thus increasing the necessary statistics. However, the important novelty is that a largely data-driven approach is followed where the background normalization is part of the fit, thus resulting in reducing the expected systematic uncertainties.

Naturally, more data will improve the statistical uncertainty but more importantly they will also provide a better understanding of the detector. A number of systematics can be therefore improved, namely the scale factors for trigger, reconstruction and identification of objects, the jet energy scale treatment which follows a largely conservative approach, similarly the b-tagging uncertainty which also depends on the amount of available data for calibrating the b-tagging algorithms. All these uncertainties are based An extension of the method can also be implemented such that it increases the number of kinematic regions, isolating parts of the phase space with a much greater signal-over-background ratio, e.g. separating the inclusive tagged regions to an exactly one b-tagged and an inclusive two b-tagged bins. This approach can increase the number of equations and therefore allow to parametrize also the b-tagging

efficiency within the model.

It is important to highlight that the analysis presented in this thesis has provided a measurement of the inclusive $t\bar{t}$ cross-section. Even though the result shows a good agreement between theory and experiment, it cannot be inferred that this agreement holds for the complete $t\bar{t}$ phase-space. As an example, a $t\bar{t}$ resonance signal may be present in the data e.g. due to gauge bosons which couple strongly to the top quark [176]. In this case, this signal will show as an excess in the $t\bar{t}$ invariant mass spectrum. Naturally, such theories cannot be excluded unless they are probed by the experiment. With the larger data sample that ATLAS is collecting will allow a more accurate measurement of the inclusive $t\bar{t}$ cross-section which will pave the way for the measurement of the differential cross-section and the discovery of such processes. What is considered our signal today is simply our background for future discoveries.

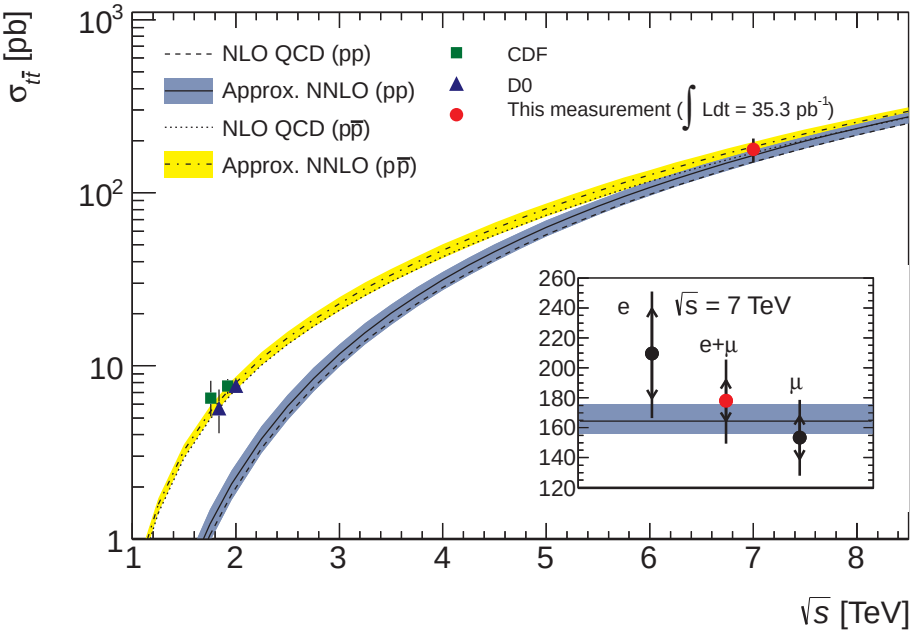

Figure 6.6: *The inclusive $t\bar{t}$ production cross-section as estimated by theory (for $M_{top} =$ 172.5 GeV) with respect to the center-of-mass energy of $p-p$ and $p-\bar{p}$ collisions (lines) [171], the measurements made from CDF, DØ during Run-I and Run-II of the Tevatron collider (square and triangle points) [174, 172, 175, 173] and the measurement performed in this thesis (circle point) with $\int \mathcal{L}dt = 35.3$ pb^{-1} of proton-proton collisions delivered by the LHC to the ATLAS detector. The error-bar region in between the arrows indicates the contribution of the statistical uncertainty only.*

Source	$\Delta\sigma/\sigma$ (%) e-channel	μ-channel	Combination
Statistical	± 14.2	± 9.2	± 7.6
	Systematics		
Object selection			
Lepton trigger, reconstruction & identification SF	± 4.0	± 1.5	± 2.5
Lepton energy scaling & resolution smearing	$+1.3/-1.2$	± 0.4	$+1.4/-1.3$
Jet energy scale	$+5.3/-6.2$	$+4.2/-5.8$	$+4.6/-6.0$
Jet energy resolution	± 1.9	± 1.8	± 1.9
Jet reconstruction efficiency	± 2.8	± 3.3	± 3.1
b-tagging calibration	$+3.3/-4.9$	$+3.5/-4.2$	$+3.5/-4.5$
Monte Carlo description			
W+jets heavy flavor content	$+5.5/-5.8$	$+7.5/-5.8$	$+6.4/-5.8$
Signal ISR/FSR	$+3.8/-4.8$	$+4.3/-5.2$	$+4.1/-5.1$
PDF	± 1.7	± 1.7	± 1.7
NLO generator	± 2.6	± 1.7	± 1.9
Parton shower	± 1.2	± 0.3	± 0.6
Pile-up activity	± 5.8	± 5.5	± 5.6
QCD normalization	$+1.4/-0.6$	$+0.3/-0.1$	$+0.5/-0.2$
Templates			
Data-driven method	± 4.1	± 3.5	± 3.7
Functional parametrization	± 1.2	± 1.2	± 1.2
Sum systematics	$+13.3/-14.5$	$+13.1/-13.4$	$+12.9/-13.8$
Statistical + Systematics	$+19.5/-20.3$	$+16.0/-16.2$	$+15.0/-15.8$
Int. Luminosity	$+3.5/-3.3$	$+3.5/-3.3$	$+3.5/-3.3$

Table 6.14: *Summary of uncertainties on the $t\bar{t}$ production cross-section for the individual channel fits and the combined channel fit.*